Nuclear Engineering and Technology 54 (2022) 1167–1174

Contents lists available at ScienceDirect

Nuclear Engineering and Technology

journal homepage: www.elsevier.com/locate/net

Original Article

Classification of ultrasonic signals of thermally aged cast austenitic stainless steel (CASS) using machine learning (ML) models

Jin-Gyum Kim [a, b], Changheui Jang [b], Sung-Sik Kang [a, *]

[a] Korea Institute of Nuclear Safety, Daejeon, 34142, Republic of Korea
[b] Department of Nuclear and Quantum Engineering, Korea Advanced Institute of Science and Technology, Daejeon, 34141, Republic of Korea

ARTICLE INFO

Article history:
Received 8 July 2021
Received in revised form
31 August 2021
Accepted 29 September 2021
Available online 4 October 2021

Keywords:
Cast austenitic stainless steel (CASS)
Thermal aging
Ultrasonic technique
Machine learning (ML)
Classification

ABSTRACT

Cast austenitic stainless steels (CASSs) are widely used as structural materials in the nuclear industry. The main drawback of CASSs is the reduction in fracture toughness due to long-term exposure to operating environment. Even though ultrasonic non-destructive testing has been conducted in major nuclear components and pipes, the detection of cracks is difficult due to the scattering and attenuation of ultrasonic waves by the coarse grains and the inhomogeneity of CASS materials. In this study, the ultrasonic signals measured in thermally aged CASS were discriminated for the first time with the simple ultrasonic technique (UT) and machine learning (ML) models. Several different ML models, specifically the K-nearest neighbors (KNN), Support Vector Machine (SVM), and Multi-Layer Perceptron (MLP) models, were used to classify the ultrasonic signals as thermal aging condition of CASS specimens. We identified that the ML models can predict the category of ultrasonic signals effectively according to the aging condition.

© 2021 Korean Nuclear Society, Published by Elsevier Korea LLC. This is an open access article under the CC BY-NC-ND license (http://creativecommons.org/licenses/by-nc-nd/4.0/).

1. Introduction

Cast austenitic stainless steels (CASSs) are austenitic stainless steels manufactured by the casting method. CASS materials are widely used in the nuclear industry because they can handle complicatedly-shaped and large-sized components with high strength, good weldability, and better stress corrosion cracking resistance [1–6]. Despite various advantages, CASS has a critical drawback of being vulnerable to thermal aging degradation (i.e. embrittlement) during the long-term exposure to operating temperatures of nuclear power plants (NPPs). The δ-ferrite of CASS generated during the casting process is in thermodynamically non-equilibrium state, and detrimental microstructure evolution could occur during the operation of NPPs, leading to decreased ductility, toughness, and fracture resistance [5]. It has been reported that the main causes of this of CASS are the Cr-rich α′-phase formed by the spinodal decomposition in δ-ferrite or the precipitation of G-phase and $M_{23}C_6$ carbide at the ferrite-austenite phase boundary [1,2]. Recently, studies have been conducted in order to elucidate the thermal aging mechanism with the comparison of the nano-scale microstructure and mechanical properties of CASS [3–6].

Components and piping materials in NPPs are exposed to the harsh environment of high temperature, pressure, and radiation, which leading to degradation of the materials. For the safety of NPPs, maintaining the integrity of these materials is critical because the integrity of materials play an important role in preventing the leakage of harmful radioactive materials to the environment. It is required that NPPs are subjected to the in-service inspection to detect the cracks which can cause leakage of coolant during operating of NPPs. Among the various non-destructive evaluation (NDE) techniques for the in-service inspection, ultrasonic testing (UT) is widely used because it can check the internal cracks of components and piping of NPPs effectively.

Recently, artificial intelligence (AI)-related techniques have been applied rapidly in researches on NDE [7–9]. In a few of these researches, machine learning (ML) techniques have been applied to study the damage and crack evaluation of materials. For example, A.R. Jac Fredo et al. classified the digital images of damage to surface of composite materials using support vector machine (SVM) classifier, and the classification accuracy was 96.6% [10]. W. Choi et al. conducted a study to classify the digital images of surface of the boiler tube as degree of material degradation using deep convolutional neural network with image processing techniques, and the classification accuracy of this network for prediction was more than

* Corresponding author.
E-mail address: sskang@kins.re.kr (S.-S. Kang).

https://doi.org/10.1016/j.net.2021.09.033
1738-5733/© 2021 Korean Nuclear Society, Published by Elsevier Korea LLC. This is an open access article under the CC BY-NC-ND license (http://creativecommons.org/licenses/by-nc-nd/4.0/).

99% [11]. N. Munir et al. applied the deep neural network to classify the ultrasonic signals of weld defects [12,13]. The network can classify the signals of defect with high accuracy and, the performance of network was improved by removing the noise using an autoencoder model [13].

The fracture toughness and the cracking resistance of CASS decreased by thermal aging, which may lead to cracking and leakage of coolant accidents. So, the NDE of CASS is essential for keeping the integrity of material. In general, the UT, one of the NDE techniques, was applied to evaluate the internal flaws in component and piping. The pulse-echo and time of flight diffraction methods were generally used to check the flaws with amplitude measurement of ultrasonic signal reflected and tip diffraction signal from flaws in material. However, it is difficult to detect flaw indications using ultrasonic techniques in CASS because of the high scattering and attenuation of ultrasonic waves induced by the inherently coarse-grained and inhomogeneous microstructure [14–16]. These scattering and attenuation of ultrasonic wave are the main causes of low probability of detection in NDE of CASS. Moreover, the small peak-to-peak (PtoP) amplitude of signals give poor discrimination for the human eye, leading to human error with missing the cracks.

Most conventional UT is focused on the crack or flaw detection, however, we tried to apply the ultrasonic technique to detect the degree of material degradation. Detecting the material degradation is in order to prevent the drastic fracture of materials having low fracture toughness such as CASS. In previous study, P. Majumdar et al. measured the elastic modulus of biomedical titanium alloys by ultrasonic technique and compared with nano-indentation data and microstructure images [17]. Also, our previous study for checking the materials degradation of CASS was conducted using the nonlinear ultrasonic technique (NUT) [18]. The nonlinear ultrasonic technique is one of the promising way to identify the material characteristics, which can discriminate the change of material by the distortion of ultrasonic wave. However, the NUT needs the elaborate experimental setup and complicated signal processing. Meanwhile, in this study, the relatively simple ultrasonic technique with ML was applied to detect and predict the category of ultrasonic signals as the degree of material degradation.

In Section 2, the material information, measurement procedures of ultrasonic waves, and preprocessing method and ML models for UT signals are described. Section 3 introduces the classification and prediction results by the ML models and discussion of the results. Lastly, a summary and conclusions are provided in Section 4.

2. Material and measurement

2.1. Material

The grade of the CASS material used in the study is CF8M. The chemical composition and delta ferrite content of CF8M are shown in Tables 1 and 2, respectively. The chemical composition of the material complied with ASTM A351 CF8M [19], and the material was made by the static casting method. These specimens were provided after thermal aging and the Charpy impact test by the Pacific Northwest National Laboratory (PNNL) in the U.S. [2], which is a part of the Program for Investigation of NDE by International Collaboration (PIONIC). Five CF8M specimens are prepared with the same width and depth (10 mm × 10 mm). The thermal aging conditions of specimens are provided in Table 3. The aging temperatures were 290 °C, 330 °C, 360 °C, and 400 °C and the aging time was 10,000 h for all specimens. It was confirmed that the specimens experience signification reduction of impact energy in a previous study [2]. Also, the maximum aging conditions of 400 °C and 10,000 h are sufficient to cause the significant spinodal decomposition of CF8M, as determined by a microstructure analysis [2,3]. In order to verify the embrittlement of CASS by spinodal decomposition, the micro-hardness in ferrite and austenite phase was measured. A Vickers hardness tester (Wolpert Wilson Instruments) was used to measure the micro-hardness in ferrite with load condition of 10 g and dwell time of 10 s. We measured three points in ferrite phase and averaged. As shown in Fig. 1, the hardness of ferrite phase increased with the degree of thermal aging, while those of austenite phase did not changed remarkably.

Table 2
δ-ferrite content of CF8M in the as-cast condition [2].

Grade	FN	STDEV(FN)	vol%	STDEV(vol%)
CF8M	4.9	0.52	5.6	0.60

2.2. Measurement of ultrasonic waves

Fig. 2 shows the experimental setup to measure the ultrasonic waves with the pulse-echo technique at one side of the specimen along the thickness of 10 mm. The ultrasonic waves are generated by a Pulser/Receiver (JSR, DPR300) and the ultrasonic transducer of 0.25" diameter with couplant gel. The center frequency of transducer is 10 MHz. The waves were visualized and collected by an oscilloscope (LeCroy, HDO4034A) with fixed gain of 16 dB of receiver.

The number of measured ultrasonic signals for each aging condition is 25 as shown in Fig. 3, therefore, 125 signals were collected as the raw signals. For each signal, 200,002 points were recorded during 20 μs, which is the sample rate of 10 GS/s (gigasamples per second). The amplitudes of signals were expressed in units of voltage in the oscilloscope. The measurement locations were randomly chosen in each sample within a horizontal range of ±5 mm at the center of the specimen. The measured signals thus show slight differences of amplitude and phase even in the same specimen. This method was applied to obtain various signals from the same specimen for reflecting the shape change of signals according to the measurement position, which uncertainties in location were intentionally introduced in order to avoid overfitting. That is, if the signals were used from the only specific location, the

Table 3
Conditions of thermal aging.

Specimen No.	Aging condition	
	Temperature	Time
1	As-cast	0 h
2	290 °C	10,000 h
3	330 °C	
4	360 °C	
5	400 °C	

Table 1
Chemical composition; amounts are given in wt% for the main alloy elements and in ppm for C, S, O, and N [2].

Grade	Fe	Cr	Ni	Mn	Mo	Si	Cu	C	S	O	N
CF8M	Bal.	18.52	10.38	0.65	2.33	1.02	0.33	433	243	207	1020

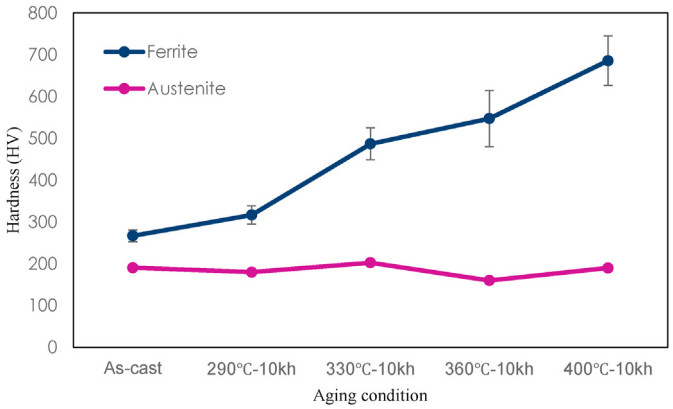

Fig. 1. Hardness of ferrite and austenite phase.

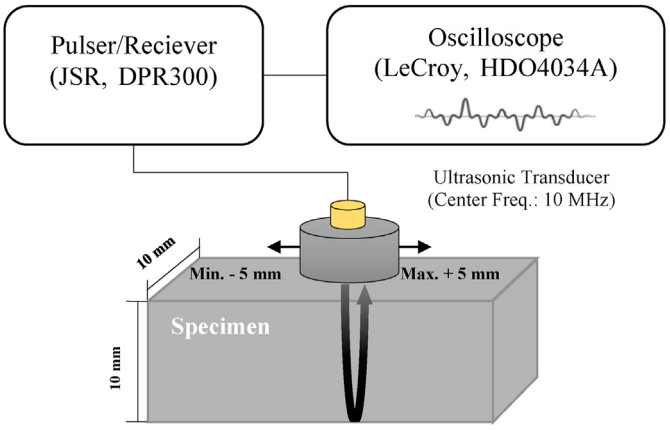

Fig. 2. Schematic diagram of ultrasonic experimental setup.

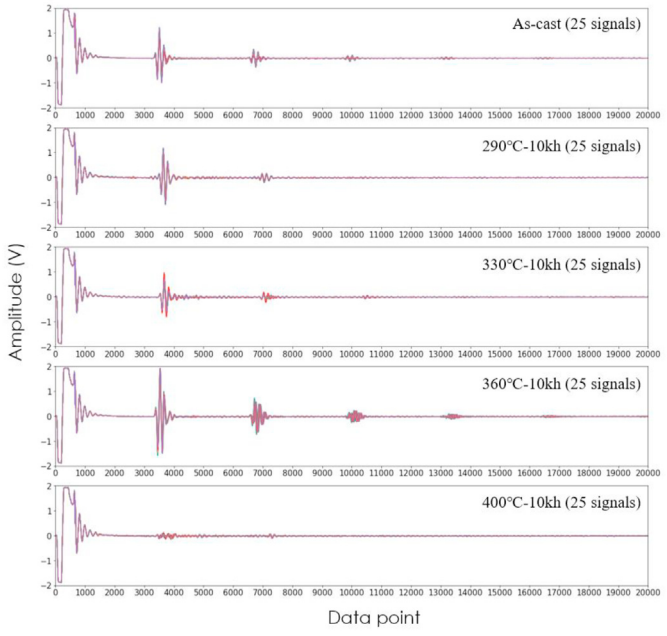

Fig. 3. Ultrasonic waves according to the aging conditions ((a) as-cast, (b) 290°C-10 kh, (c) 330°C-10 kh, (d) 360°C-10 kh, (e) 400°C-10 kh)

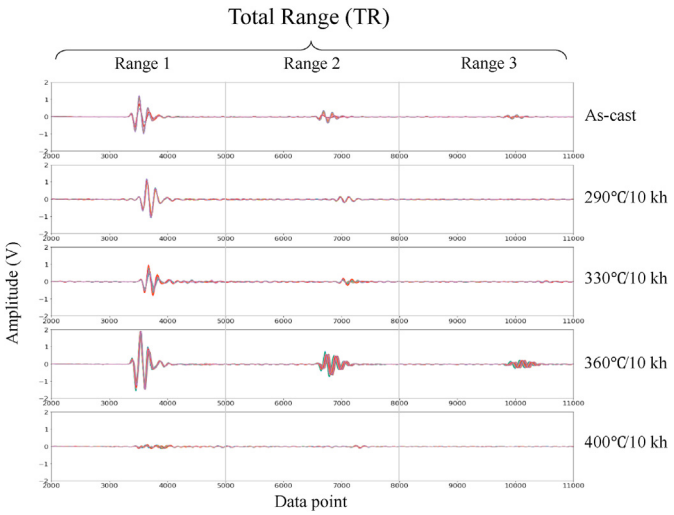

Fig. 4. Ultrasonic signals with respect to the range and aging condition.

ML system would not classify the signals of other location correctly even in the same specimen.

2.3. Pre-processing of ultrasonic signals

It is important to properly process the input data for an efficient ML analysis. In this study, the collected raw UT signals were down-sampled while minimizing the loss of original information. If the ML analysis were performed using the raw signals of 200,002 points, it would be inefficient because the computation time for learning would be too long. Therefore, it was down-sampled to 20,000 points, which is 1/10 of the raw signals. This level yields about 1 GS/s sampling performance, which is sufficient to represent the information of signals by the 10 MHz transducer. When the ML system performed classification, time information was not essential, and hence it was used only the amplitude value assigned to each point. In Fig. 4, the range of signals for ML analysis is chosen from the 2000th point up to the 11,000th point of the down-sampled data, which includes 1st-3rd reflection signals from back of the sample. The front parts (data point range of 0–2000) of signals were excluded to remove the part of signals caused by coupling effect of transducer-material and augment the signals with phase shift of X-axis. This is the total range (TR) of signals for ML analysis in this study.

The TR is divided into three sub parts with every 3000 points, such that each part contains one reflection signal; Range 1, Range 2, and Range 3, as described in Fig. 4. The reason for dividing the range is to check the impacts of major information of signals such as PtoP

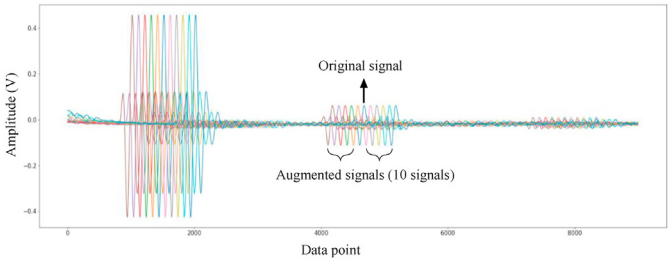

Fig. 5. Example of augmented signals of TR with phase shifting.

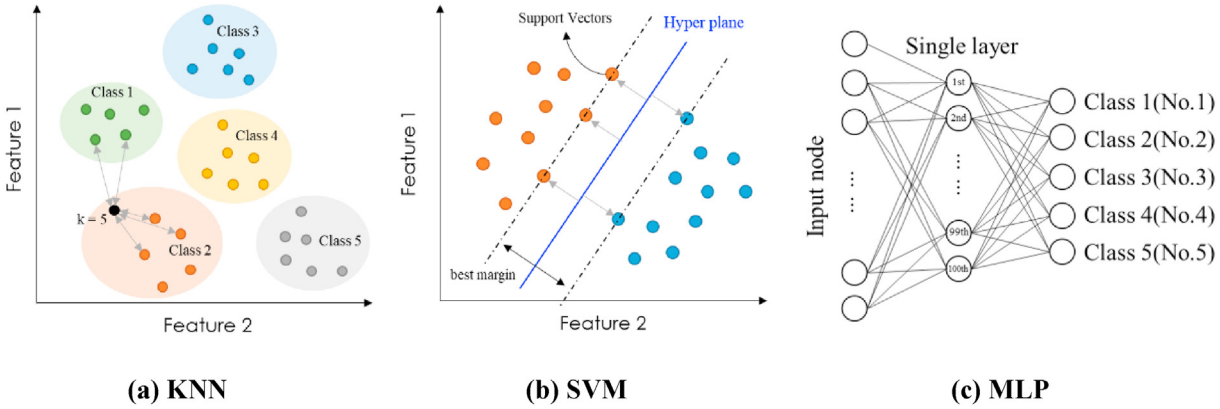

Fig. 6. Conceptual diagrams of ML models ((a) KNN, (b) SVM, (c) MLP).

amplitude on the classification performance when the trained models classify the test data. That is, although the signals may have relatively smaller amplitude like Range 3, which would be difficult to classify by human eye, we would like to check whether the ML models can classify the signals effectively according to the aging conditions. The average values of the PtoP amplitude of 125 signals in Range 1, Range 2, Range 3 are 1.743 V, 0.4676 V, and 0.1499 V. In Range 3, the PtoP amplitude is relatively small. In particular, in the cases of No.2 (290°C-10 kh) and No.5 (400°C-10 kh) specimens, the negligible reflected signal can be seen.

To augment the number of training and test samples, the phase shifting of the signals was applied [9]. In this study, the phase of the original signals of each range was shifted every 100 points from minimum of −500 points to maximum of +500 points, so the one signal was augmented to 11 signals. The results of augmentation to the TR are given in Fig. 5. Considering that the total number of data points is 20,000, a maximum phase difference is 5% (1000 points) of down-sampled signals. Finally, the down-sampled signals were augmented from 125 signals to 1375 signals to each ranges, so the four datasets (TR, Range 1, Range 2, Range 3) were prepared. All datasets were split into training datasets of 825 signals (60%) and test datasets of 550 signals (40%). All data were processed using the Standard Scaler, which is one of the calculation modules for standardization in Scikit-learn [20].

2.4. Machine learning models

Three classification models were used: K-nearest Neighbors (KNN) [21], Support Vector Machine (SVM) [22,23], and Multi-Layer Perceptron (MLP) [24–26]. These models were operated in Scikit-learn with default settings [27]. Conceptual diagrams of ML models are shown in Fig. 6.

2.4.1. K-nearest neighbors

KNN is the one of the fundamental classification models. It is based on the Euclidean distance between a test sample and the training samples as shown in Fig. 6a [21]. KNN can decide the class of test sample by the nearest neighbor's class of training sample. The value of n_neighbors was set 5, which means that the test data are classified using the 5 nearest data around the test data of one feature.

Model Summary 1

```
>>> from sklearn.neighbors import KNeighborsClassifier
>>> model = KNeighborsClassifier(n_neighbors=5)
>>> model.fit(X_train, y_label)
```

2.4.2. Support vector machine

SVM is a ML model to solve the two-class problems by hyperplane and support vector as shown in Fig. 6b [22]. We set the regularization parameter C of 1.0 which is inversely proportional to the strength of the regularization. As increasing the strength of regularization, the model tries to focus not individual datum but the trend of data distribution. The kernel of SVC was the radial basis functional kernel (RBF) for performing the nonlinear classification. The decision function shape was set the one-vs-one (ovo), therefore 10 classifiers are constructed in this study [23].

Model Summary 2

```
>>> from svm import SVC
>>> model = SVC(C=1.0, kernel = 'rbf', decision_function_shape = 'ovo')
>>> model.fit(X_train, y_label)
```

2.4.3. Multi-Layer Perceptron

MLP network is a basic neural network composed of N-dimensional input and M-dimensional output with a hidden layer and the use of the back propagation learning model as shown in Fig. 6c [24]. We used a single layer network with 100 nodes. The activation function of model is Rectified Linear Unit (ReLU) [25], and Adam optimizer was applied in this model [26].

Model Summary 3

```
>>> form sklearn.neural_network import MLPClassifier
>>> model = MLPClassifier(hidden_layer_sizes=100, activation='relu', solver='adam')
>>> model.fit(X_train, y_label)
```

3. Results and discussion

In order to check the classification performance of the ML models, we analyzed the accuracy of the ML model using training and test datasets. The accuracy is the rate of the number of correctly predicted samples out of all the samples [28]. For the training datasets of 825 signals, we identified the accuracy of ML models by the cross-validation (CV). The CV is a resampling method to datasets that uses multiple training and validation sets, and it is applied to describe the classification performance of ML models [29]. In this study, the ten-fold CV was conducted as shown in Fig. 7. The average accuracies and standard deviation by CV are shown in Table 4 and Fig. 8.

Even with the standard deviation, the results showed that the classification accuracies of ML models were above 95%. It means that the ML models can classify the signals of thermally aged CASS specimens accurately according to the aging condition. In the case of Range 1, which have the highest PtoP amplitudes among the signals, the classification accuracies are relatively high compared to other ranges. In this case, SVM, KNN, and MLP show good classification performance in the order. For the SVM, the standard deviation is 0, which shows the best validation results. However, in Range 2 and Range 3 where the PtoP value is not large, the classification performance of both KNN and SVM decreased and the standard deviation of accuracies increased significantly. Meanwhile, for Range 2 and Range 3, the MLP performance was the best. The MLP results showed relatively similar performance with Range 1, Range 2 and Range 3, which indicates that the signals for each aged condition could be well classified regardless of the amplitude differences. In particular, the signals of Range 3 can be classified with the accuracy of above 97% through the MLP despite the very small PtoP amplitude.

Another performance validation was attempted with a test datasets of 550 signals which was never used in training. These signals are arbitrarily taken from augmented signals (1375 signals), and the number of signals for each class is randomly distributed. The accuracy results of the ML models to the test datasets are shown in Table 5 and Fig. 9.

Like the CV results, the accuracies to test dataset was as high as 96% or more for all ranges. For the TR and Range 1, KNN predicted them with 100% accuracy. It was also confirmed that the accuracy of SVM and MLP was more than 99%. However, in Ranges 2 and 3, the performances of ML models decreased slightly, and for the KNN, the greatest performance reduction was seen among the models. For the signals having differences clearly such as total and range 1, the KNN model shows good performance to predict the data using the distance from the learned data nearby, however, it was identified that the KNN model has poor performance for signals having subtle changes. Although these reduction of performance, the accuracies of three models were above 96%. The accuracy of the test datasets has a limitation to represent the performance of the system because it is a result obtained from the test dataset of ranges as one dataset. Nonetheless, it is meaningful to evaluate the prediction performance of the ML model with dataset not used for training. Fig. 10–13 show the confusion matrix of the test dataset according to the ranges, which were drawn by Scikit-learn [21,30]. The confusion matrices provide detailed results that the ML models had predicted the data. The values in the confusion matrix are the number of signals for each class and the values of diagonal terms indicate the number of correctly predicted signals.

In order to verify the test dataset with another approach, the F-1 score was calculated. The F-1 score is the harmonic mean of recall and precision, as defined in equations (1-3) [31]. When the number of signals of each class is not balanced in the dataset, the F-1 score is useful to evaluate the performance of prediction. The F-1 scores of ML models are shown in Table 6. All the models show the high F-1 score close to the 1.0 in prediction the signals of thermally aged specimens. In Range 2 and 3, it is identified that the prediction performance of KNN and SVM slightly decreased.

$$\mathrm{F}-1\ \mathrm{score} = 2 \times \frac{\mathrm{precision} \times \mathrm{recall}}{\mathrm{precision} + \mathrm{recall}} \tag{1}$$

$$\mathrm{precision} = \frac{\mathrm{True\ Positive}}{\mathrm{True\ Positive} + \mathrm{False\ Positive}} \tag{2}$$

$$\mathrm{recall} = \frac{\mathrm{True\ Positive}}{\mathrm{True\ Positive} + \mathrm{False\ Negative}} \tag{3}$$

In summary, all three models showed excellent classification

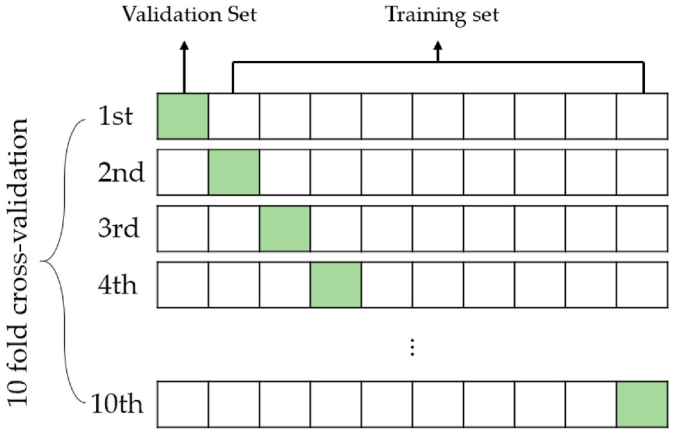

Fig. 7. Conceptual diagram of cross-validation with 10 folds of training datasets.

Table 4
Average accuracy and standard deviation by CV for training dataset.

Models	Average Accuracy				Standard Deviation			
	TR	Range 1	Range 2	Range 3	TR	Range 1	Range 2	Range 3
KNN	0.9976	0.9988	0.9818	0.9660	0.0048	0.0036	0.0125	0.0152
SVM	1	1	0.9830	0.9758	0	0	0.0181	0.0152
MLP	0.9915	0.9927	0.9818	0.9842	0.0077	0.0124	0.0136	0.0134

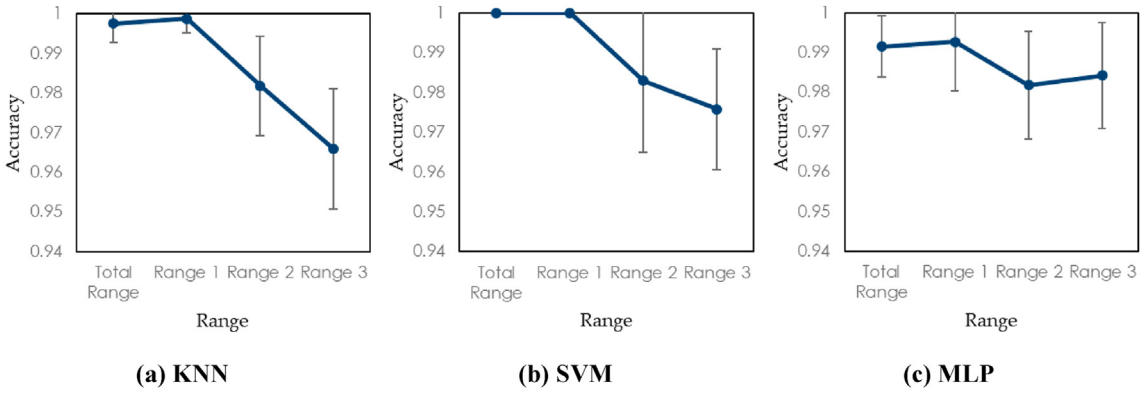

Fig. 8. Accuracies of ML models to the training dataset by cross-validation ((a) KNN, (b) SVM, (c) MLP).

Table 5
Accuracy of classification to test dataset.

Models	TR	Range 1	Range 2	Range 3
KNN	1	1	0.9982	0.9636
SVM	0.9982	0.9964	0.9836	0.9836
MLP	0.9909	0.9964	0.9927	0.9854

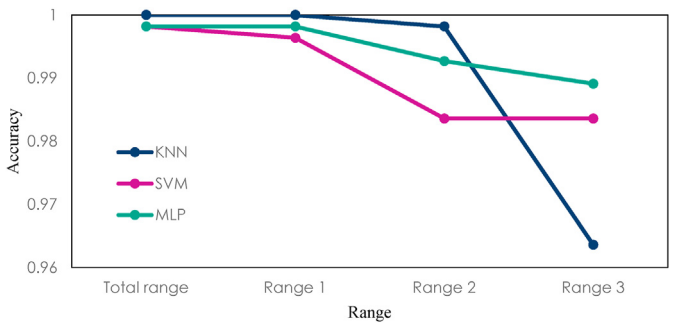

Fig. 9. Accuracies of ML models to the test dataset.

and prediction performance of above 95%. Through these results, the feasibility of prediction for detecting the degree of thermal aging of CASS was confirmed using the ultrasonic signals and ML models. The KNN and SVM showed better performance than MLP when the signals (TR & Range 1) have larger PtoP amplitude than Range 2 and 3, whereas the MLP was useful for classifying signals (Range 3) whose PtoP amplitude is smaller than those of others. Previously, the subtle microstructure changes due to thermal aging in CASS can be identified using transmission electron microscope with nano-scale resolution [3,6]. It is possible that these subtle changes may distort the UT signals slightly, though they could not be distinguished by human eye. However, considering the classification results of Range 3 signals, the ML models can classify the subtle difference of signals very well. Especially, the MLP series models appeared to be more suitable to evaluate and classify the slight change in ultrasonic signals by thermal aging.

In the CASS materials, the shape of ultrasonic signals was affected significantly due to the high scattering and attenuation by inherent coarse grains. The degree of these effects is irregular and unpredictable because of the complexity of microstructure. In addition, the subtle changes of signals are caused by thermal aging

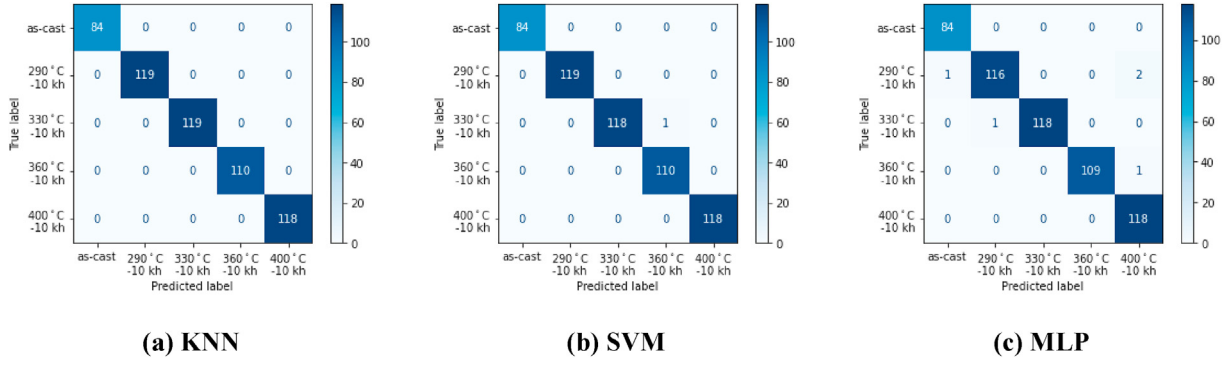

Fig. 10. Confusion matrix to the test dataset of TR ((a) KNN, (b) SVM, (c) MLP).

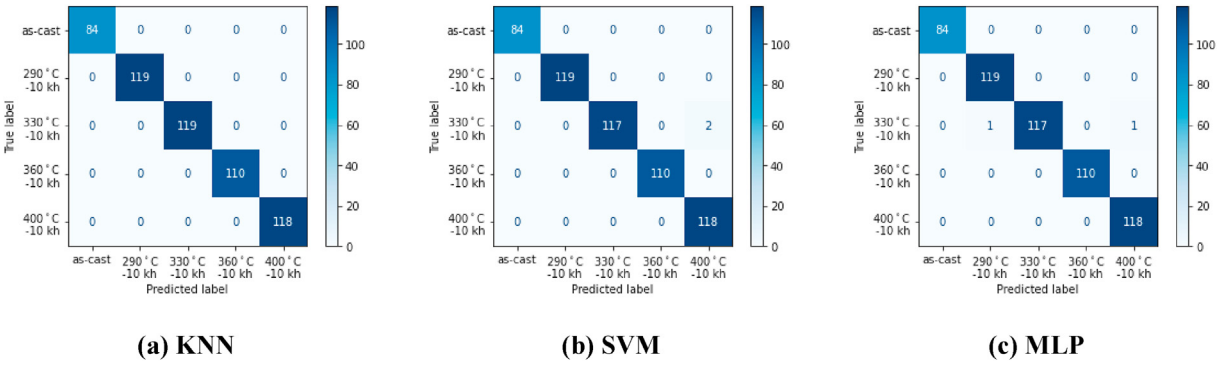

Fig. 11. Confusion matrix to the test dataset of Range 1 ((a) KNN, (b) SVM, (c) MLP).

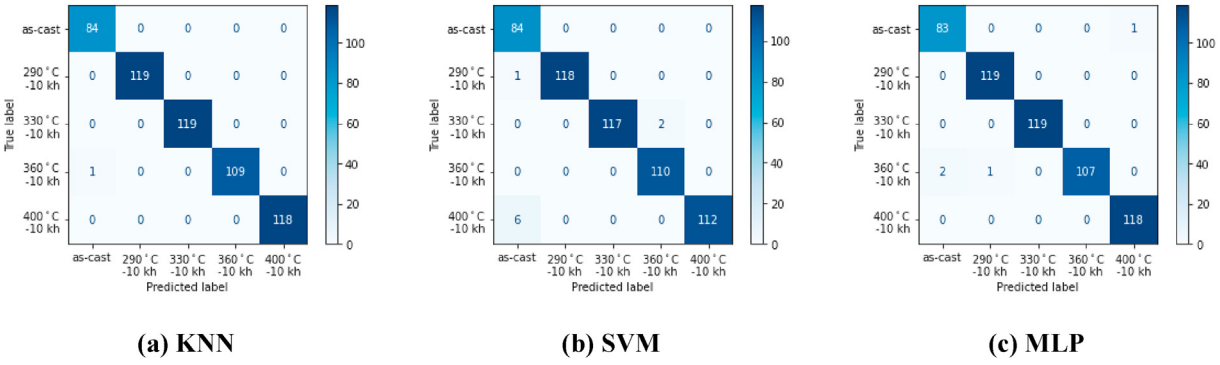

Fig. 12. Confusion matrix to the test dataset of Range 2 ((a) KNN, (b) SVM, (c) MLP).

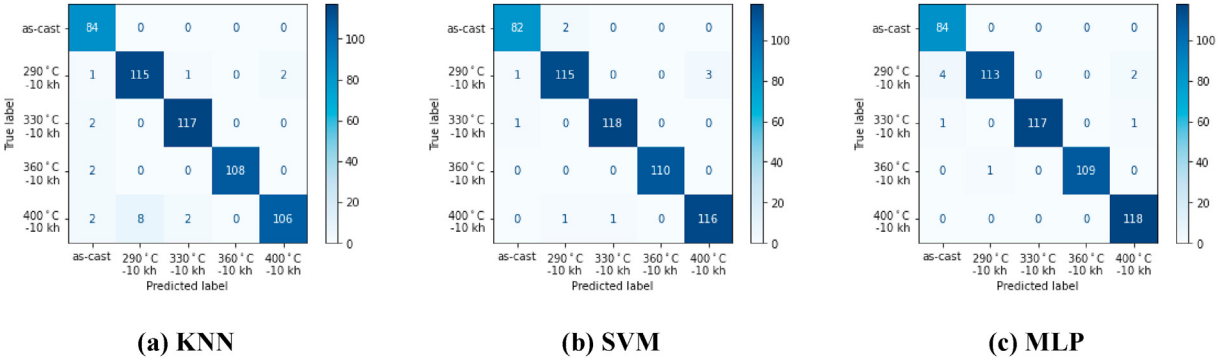

Fig. 13. Confusion matrix to the test dataset of Range 3 ((a) KNN, (b) SVM, (c) MLP).

Table 6
F-1 scores of ML models.

	Total	Range 1	Range 2	Range 3
KNN	1	1	1	0.96
SVM	1	1	0.98	0.98
MLP	0.99	0.99	0.99	0.99

mechanism, which are very difficult to distinguish by conventional UT. Under these limitations, the results show that the ML models have potential to discriminate the subtle change of UT signals. On the other hand, it appears that an interpretable ML model is necessary in order to investigate the correlation between the change in the microstructure and in the ultrasonic signal with respect to the degree of thermal aging.

4. Conclusions

In this study, ML models were applied for the first time to classify and predict the ultrasonic signals as degree of thermal aging of CASS used in NPPs. The ultrasonic signals obtained from the thermally aged CASS specimens were effectively classified and predicted with an accuracy of above 95% using ML models. This shows the possibility of classifying and predicting the CASS thermal aging phenomenon using NDE techniques. To verify the accuracy of the ML models, quantitative comparisons were performed using cross-validation and F-1 score. For signals having large PtoP amplitude, KNN and SVM showed higher classification performance than MLP, while for signals having small PtoP amplitude,MLP showed better performance. Though the microstructure changes due to thermal aging were expected to be very subtle, and

the changes in the ultrasonic signals would be slight, it was shown that the MLP model could accurately classify and predict the signals of thermally aged CASS materials.

Declaration of competing interest

The authors declare that they have no known competing financial interests or personal relationships that could have appeared to influence the work reported in this paper.

Acknowledgement

This study was supported by the Korea Foundation of Nuclear Safety (KoFONS) using financial resources granted by the Nuclear Safety and Security Commission (NSSC) of the Republic of Korea. (No. 2106001). The thermally aged CASS specimens were provided by the PNNL as a part of an international collaborative R&D project of PIONIC. We wish to thank Dr. Jongbeom Kim, Dr. Kyung-Mo Kim (Korea Atomic Energy Research Institute, KR) who helped us in providing the ultrasonic equipment. Also, we would like to acknowledge Dr. Thak Sang Byun (Oak Ridge National Laboratory, US) who helped us in providing the information of specimens.

References

[1] O.K. Chopra, A. Sather, Initial assessment of the mechanisms and significance of low-temperature embrittlement of cast stainless steels in LWR system. Nuclear Regulatory Commission, 1990. NUREG/CR-5385.
[2] H.M. Chung, Aging and life prediction of cast duplex stainless steel components, Int. J. Pres. Ves. Pip. 50 (1–3) (1992) 179–213.
[3] H. Jang, S. Hong, C. Jang, J.G. Lee, The effects of reversion heat treatment on the recovery of thermal aging embrittlement of CF8M cast stainless steels, Mater. Des. 56 (2014) 517–521.
[4] C. Jang, H. Jang, S. Hong, J.G. Lee, Evaluation of the recovery of thermal aging embrittlement of CF8M cast stainless steels after reversion heat treatments, Int. J. Pres. Ves. Pip. 131 (2015) 67–74.
[5] T.S. Byun, D.A. Collins, T.G. Lach, E.L. Carter, Degradation of impact toughness in cast stainless steels during long-term thermal aging, J. Nucl. Mater. 542 (2020) 152524.
[6] B. S. Kong, C. Jang, S. Kang, T. S. Byun, Evaluation of thermal ageing of cast austenitic stainless steels – mechanical properties in micro- and macro-scale, in: Proceedings of the 13th International Symposium on the Integrity of Nuclear Components, Virtual Meeting, April 21-22, 2021.
[7] C. Wunderlich, C. Tschöpe, F. Duckhorn, Advanced methods in NDE using machine learning approaches, in: AIP Conference Proceedings, 1, 2018, 020022.
[8] J.B. Harley, D. Sparkman, Machine learning and NDE: past, present, and future, in: AIP Conference Proceedings, 2102, 2019, 090001.
[9] P. Gardner, R. Fuentes, N. Dervilis, C. Mineo, S.G. Pierce, E.J. Cross, K. Worden, Machine learning at the interface of structural health monitoring and non-destructive evaluation, Philosophical Transactions of the Royal Society A 378 (2182) (2020) 20190581.
[10] A.J. Fredo, R.S. Abilash, R. Femi, A. Mythili, C.S. Kumar, Classification of damages in composite images using Zernike moments and support vector machines, Compos. B Eng. 168 (2019) 77–86.
[11] W. Choi, H. Huh, B.A. Tama, G. Park, S. Lee, A neural network model for material degradation detection and diagnosis using microscopic images, IEEE Access 7 (2019) 92151–92160.
[12] N. Munir, H.J. Kim, S.J. Song, S.S. Kang, Investigation of deep neural network with drop out for ultrasonic flaw classification in weldments, J. Mech. Sci. Technol. 32 (7) (2018) 3073–3080.
[13] N. Munir, J. Park, H.J. Kim, S.J. Song, S.S. Kang, Performance enhancement of convolutional neural network for ultrasonic flaw classification by adopting autoencoder, NDT E Int. 111 (2020) 102218.
[14] P. Jeong, F. Ammirato, Ultrasonic examination of cast stainless steel component in nuclear power plant. Review of Progress in Quantitative Nondestructive Evaluation, 1989, pp. 2105–2112.
[15] P. Ramuhalli, et al., Ultrasonic Characterization of Cast Austenitic Stainless Steel Microstructure: Discrimination between Equiaxed-And Columnar-Grain Material–An Interim Study, Pacific Northwest National Lab.(PNNL), 2009. PNNL-18912.
[16] R.E. Jacob, et al., NDE Reliability Issues for the Examination of CASS Components, Pacific Northwest National Lab.(PNNL), 2019. PNNL-28840.
[17] P. Majumdar, S.B. Singh, M. Chakraboty, Elastic modulus of biomedical titanium alloys by nano-indentation and ultrasonic techniques – a comparative study, Mater. Sci. Eng. 489 (2008) 419–425.
[18] J. Kim, J.G. Kim, B. Kong, K.M. Kim, C. Jang, S.S. Kang, K.Y. Jhang, Applicability of nonlinear ultrasonic technique to evaluation of thermally aged CF8M cast stainless steel, Nuclear Engineering and Technology 52 (3) (2020) 621–625.
[19] ASTM A351/A351M-00, Standard Specification for Castings, Austenitic, Austenitic-Ferritic (Duplex), for Pressure-Containing Parts, ASTM International, West Conshohocken, PA, USA, 2000.
[20] L. Buitinck et al., API Design for Machine Learning Software: Experiences from the Scikit-Learn Project. arXiv. 2015. https://arxiv.org/abs/1309.0238.
[21] L.E. Peterson, K-nearest neighbor, Scholarpedia 4 (2) (2009) 1883.
[22] W.S. Noble, What is a support vector machine? Nat. Biotechnol. 24 (12) (2006) 1565–1567.
[23] Scikit-learn (support vector machine), Available online: https://scikit-learn.org/stable/modules/svm.html#svm-mathematical-formulation. (Accessed 7 July 2021).
[24] M.W. Gardner, S.R. Dorling, Artificial neural networks (the multilayer perceptron) - a review of applications in the atmospheric sciences, Atmospheric environment 32 (14–15) (1998) 2627–2636.
[25] V. Nair, G.E. Hinton, Rectified linear units improve restricted Boltzmann machines, in: Haifa Icml (Ed.), Israel, 2010. June 21-24.
[26] D. P. Kingma, J. Ba, Adam: A Method for Stochastic Optimization. arXiv. 2014. https://arxiv.org/abs/1412.6980.
[27] F. Pedregosa, et al., Scikit-learn: machine learning in Python, J. Mach. Learn. Res. 12 (2011) 2825–2830.
[28] DeepAi, Available online: https://deepai.org/machine-learning-glossary-and-terms/accuracy-error-rate. (Accessed 7 July 2021).
[29] G. Zhang, M.Y. Hu, B.E. Patuwo, D.C. Indro, Artificial neural networks in bankruptcy prediction: general framework and cross-validation analysis, Eur. J. Oper. Res. 116 (1) (1999) 16–32.
[30] Scikit-learn (Confusion matrix). Available online: https://scikit-learn.org/0.18/auto_examples/model_selection/plot_confusion_matrix.html. (Accessed 7 July 2021).
[31] C. Goutte, E. Gaussier, A probabilistic interpretation of precision, recall and F-score, with implication for evaluation. European Conference on Information Retrieval, 2005, pp. 345–359.